Electrocatalytic oxidation of glycerol on Pt/C in anion-exchange membrane fuel cell: Cogeneration of electricity and valuable chemicals

Zhiyong Zhang, Le Xin, Wenzhen Li*

Department of Chemical Engineering, Michigan Technological University, Houghton, MI 49931, USA

ABSTRACT

Electrocatalytic oxidation of glycerol for cogenerating electricity and higher-valued chemicals on a Pt/C anode catalyst (2.4 nm) in an anion-exchange membrane fuel cell (AEMFC) was investigated. The peak power density of an anion-exchange membrane – direct glycerol fuel cell (AEM-DGFC) with 1.0 mg$_{Pt}$ cm^{-2} anode and non-PGM catalyst cathode can reach 124.5 mW cm^{-2} at 80 °C and 58.6 mW cm^{-2} at 50 °C, while the highest selectivity of C$_3$ acids (glyceric acid + tartronic acid) can reach 91%. The study found that higher pH reaction media could enhance fuel cell output power density (electricity generation) and selectivity of C$_3$ acids, while lower glycerol concentration could improve the selectivity of deeper-oxidized products (mesoxalic acid and oxalic acid). The fuel cell reactor with the Pt/C anode catalyst demonstrated an excellent reusability, and successfully obtained tartronic acid with a selectivity of 50% and mesoxalic acid with a selectivity of 7%, which are high compared to heterogeneous catalytic glycerol oxidation in batch reactors. It is found that the anode overpotential can regulate the oxidation product distribution, and that higher anode overpotentials favor C—C bond breaking, thus lowering the C$_3$ acids selectivity. The reaction sequence of glycerol electro-oxidation detected in an electrolysis half cell with an on-line sample collection and off-line HPLC analysis agrees with the results obtained from single fuel cell tests. However, inconsistencies between the two systems still exist and are possibly due to different reaction environments, such as electrode structure, glycerol:catalyst ratio, and residence time of reactants.

© 2012 Elsevier B.V. All rights reserved.

1. Introduction

Highly efficient catalytic processes are essential for biomass refinery into cost-competitive energy or valuable chemicals [1–3]. Selective catalytic oxidation of biomass-derived polyols is of fundamental importance in many fine chemical production processes. Glycerol (0.3 US$ kg^{-1}, crude glycerol [4]), which can be massively obtained as a byproduct of blooming biodiesel production, has great potential to serve as a main building block for future productions of higher-valued oxygenated chemicals, including glyceric acid, tartronic acid, mesoxalic acid and glycolic acid, etc. [5,6]. However, at present these value-added oxygenates are mostly produced through either costly and non-environment-friendly stoichiometric oxidation processes [7], or slow fermentation processes with low product yields [8].

To replace these out-of-date processes, extensive researches have been carried out on selective oxidation of glycerol through "green" and fast heterogeneous catalysis using molecular oxygen with mono-metallic catalysts, such as Pt [7,9–13], Pd [7,9–11,14,15], and Au [7,11,14–25], and multi-metallic catalysts,

such as PtPd [26], PtAu [27–29], AuPd [14,28,30–33], PtBi [34,35], PtCu [36], and PtPdBi [37]. It has been found that the activity and product distribution of glycerol oxidation depend on both the catalyst, such as particle size, loading, support, etc. and the reaction conditions, such as pH, glycerol:catalyst ratio, O$_2$ pressure, etc. Gallezot and co-workers studied glycerol oxidation on Pt and Pd at different pH and observed that the initial glycerol oxidation rate increased significantly with increased pH of reaction media on both catalysts [9,10,38]. They also found that the oxidation of primary –OH is more favorable than that of secondary –OH in alkaline solutions. Groups of Hutchings and Prati separately studied glycerol oxidation on Au and achieved very high selectivity to glyceric acid under their optimized conditions [16,17]. Hutchings and co-workers also investigated the effects of O$_2$ pressure and catalyst loading on glycerol oxidation on Pt/C in basic environments, and found that lower O$_2$ pressure and higher catalyst loading favor the oxidative cleavage of C—C bonds in glycerol and reaction intermediates to yield C$_1$ products [7]. Despite great progress in the oxidation of glycerol, previous researches were heavily focused on selective oxidation of one hydroxyl group of glycerol to glyceric acid or dihydroxyacetone, and breaking C—C bond of glycerol to glycolic acid. Glyceric acid is the only C$_3$ product that has shown high selectivity through heterogeneous catalysis in alkaline media. It is hard to obtain further oxidized C$_3$ products (tartronic acid and mesoxalic

acid). The published selectivity of tartronic acid is always <30% [7]. Mesoxalic acid has rarely been reported as a product from catalytic oxidation of glycerol on the metallic catalysts in batch reactors in high pH media.

Recently, Davis and co-workers' elegant work revealed the roles of OH$^-$ and O$_2$ on metallic catalyst (Au or Pt) surfaces based on HPLC–MS analysis, ^{18}O isotope tracing, and DFT calculation [23]. They found that OH$^-$ in the reaction media could greatly facilitate glycerol oxidation, and the role of O$_2$ is simply to facilitate the OH$^-$ regeneration loop via a 2-electron-transfer process on Au (or a 4-electron-transfer process on Pt). The function of O$_2$ in heterogeneous catalytic oxidation of glycerol is similar to the O$_2$ reduction reaction (ORR) at the fuel cell cathode. However, due to restrictions in the design and nature of traditional batch reactors, the chemical energy stored in glycerol (6.3 kWh L^{-1}) has been wasted in the catalytic oxidation process (it is just converted to heat in the oxidation). From energy conservation, economy, and environment aspects, it is desirable to develop new catalytic process to cogenerate both energy and value-add chemicals from these biorenewable compounds.

Glycerol has been considered a promising fuel for direct alcohol fuel cells (DAFC), due to its relatively low price, simple purification and storage, and non-volatile and environment-friendly properties [39–42]. Matsuoka et al. first investigated glycerol as fuel in an anion-exchange membrane fuel cell (AEMFC) with PtRu/C anode catalyst, and obtained a maximum power density of ~7 mW cm^{-2} at 50 °C [43]. Later, Bambagioni et al. expanded the anode catalyst to Pd/MWCNT in an anion-exchange membrane direct glycerol fuel cell (AEM-DGFC), and observed a peak power density of ~6 mW cm^{-2} in a passive fuel cell (room temperature) and a peak power density of ~80 mW cm^{-2} in an active fuel cell (80 °C) [44]. Bianchini and Shen further reported an AEM-DGFC performance of ~118 mW cm^{-2} on a Pd-(Ni-Zn-P)/C anode (80 °C) [39]. Ilie et al. optimized the membrane electrode assembly (MEA) fabrication method and reaction conditions (i.e. fuel composition, fuel flow rate, etc.), and demonstrated an AEM-DGFC peak power density of ~24 mW cm^{-2} with Pt and Pt-based bimetallic anode catalysts at 60 °C [45]. However, most previous research efforts targeted at fully oxidization of glycerol to achieve high fuel cell output power density and high Faradic efficiency, while exploring selective (partial) oxidation of glycerol to produce valuable chemicals and investigating the glycerol electro-oxidation behaviors (product distribution) on metallic catalysts in real AEMFC are ignored.

In this article, cogeneration of electricity and higher-valued chemicals from glycerol electrocatalytic oxidation was successfully achieved in single AEMFC by separating the O$_2$ reduction reaction (cathode) from the glycerol catalytic oxidation (anode). Carbon supported Pt nanoparticles (1–4 nm) served as the catalyst for glycerol electro-oxidation [46–51], which not only demonstrated decent electricity generation performance (124.5 mW cm^{-2} at 80 °C), but also showed unique catalytic selectivity towards higher-valued chemicals, such as glyceric acid, glycolic acid, and tartronic acid. It is interesting to find that the fuel cell operation voltage (anode overpotential) could regulate the product distributions. In addition, the fully oxidized C$_3$ acid, mesoxalic acid, was directly produced in this alkaline cogeneration system.

2. Experimental

2.1. Preparation of Pt/C catalysts

Pt/C catalyst was synthesized through a solution phase-based nanocapsule method [49–52]. In detail, 196.7 mg Pt(acac)$_2$ (0.5 mmol, Acros Organics) 200 μl oleylamine (OAm, Aldrich Chemistry), and 200 μl oleic acid (OAc, Fisher Chemical) were dissolved in a mixture of 146.3 mg carbon black (Vulcan XC-72R, Cabot) and 40 ml benzyl ether (Acros Organics, 99%) at 60 °C in an inert N$_2$ atmosphere. As the temperature increased to 120 °C, 1.0 ml LiBEt$_3$H (1 M in THF, Acros Organics) was quickly injected into the system. The temperature was held constant for 30 min, and then slowly increased to 180 °C and held for an additional 30 min. The final Pt/C catalyst (40 wt%) was obtained by filtration, washed with copious ethanol, and dried in a vacuum oven at 50 °C overnight.

2.2. Characterizations

X-ray diffraction (XRD) pattern of Pt/C catalyst was collected using a Scintag XDS-2000 θ/θ diffractometer with Cu K$_\alpha$ radiation ($\lambda = 1.5406$ Å), with a tube current of 35 mA and a tube voltage of 45 kV. Transmission electron microscopy (TEM) was performed by JEOL 2010 with an operation voltage of 200 kV in order to analyze the morphology of Pt/C. The Pt particle size distribution was evaluated by 100 randomly chosen particles in an arbitrary area.

2.3. MEA fabrication and electro-oxidation of glycerol in AEM-DGFC

The MEA was assembled with a Pt/C-based anode, Tokuyama A201 membrane (28 μm) and a non-Pt group metal (PGM) catalyst-based cathode. To prepare the anode, catalyst ink containing 90 wt% of as-prepared Pt/C catalyst (40 wt%) and 10 wt% of Teflon was sprayed on a carbon cloth anode diffusion layer to obtain a catalyst loading of 1.0 mg$_{Pt}$ cm^{-2}. On the cathode, a commercial non-PGM HYPERMEC^{TM} catalyst (Fe-Cu-N$_4$/C, Acta) was blended with AS-4 anion conductive ionomer (Tokuyama), and sprayed directly onto the A201 membrane to obtain a catalyst loading of 1.0 mg cm^{-2}, and was covered with a 25CC carbon paper (SGL Group) cathode gas diffusion layer. The MEA was mounted in a fuel cell with an active cross-sectional area of 5 cm^2, and tested by a Scribner-Associates 850e fuel cell test system. The electricity generation performances were evaluated with a 2.0 M KOH + 1.0 M glycerol solution and high-purity O$_2$ (99.999%) at a constant flow rate of 0.4 l min^{-1} under 30 psi back pressure, at 50 and 80 °C. The glycerol oxidation was performed by looping 55 ml of glycerol alkaline electrolyte from the anode fuel vessel into the anode plate channels at 50 °C with the same O$_2$ flow rate under 30 psi back pressure for 2–6 h. During the glycerol oxidation test, the anode overpotential was monitored with a Hg/HgO/1.0 M KOH electrode, and reported vs. standard hydrogen electrode (SHE) for convenience. After each test, 0.5 ml sample was collected from the anode fuel vessel for HPLC analysis. All the investigated products are in their deprotonated (salt) forms in alkaline media, however, we reported them in their acid forms throughout the paper.

2.4. Electro-oxidation of glycerol in half cell with on-line sample collection

The half cell test was conducted in a conventional three-electrode-cell setup, with a glassy carbon working electrode, a Hg/HgO reference electrode and a Pt wire counter electrode, at room temperature. Before each test, 2.0 mg of Pt/C catalyst were dispersed in 1.0 ml isopropanol by sonication to form a uniform ink. The working electrode was prepared by dropping 40 μl of the ink onto the glassy carbon electrode. 20 μl of 0.05 wt% AS-4 anion conductive ionomer solution was then added on the top to affix the catalyst. To analyze the glycerol oxidation sequence, linear staircase scans with increments of 100 mV 10 min^{-1} were carried out in both 0.1 M KOH + 0.1 M glycerol and 1.0 M KOH + 1.0 M glycerol solutions. Inspired by the on-line sample collection off-line HPLC analysis system reported in references [53–55], the instant reaction products under different potentials were collected on-line through
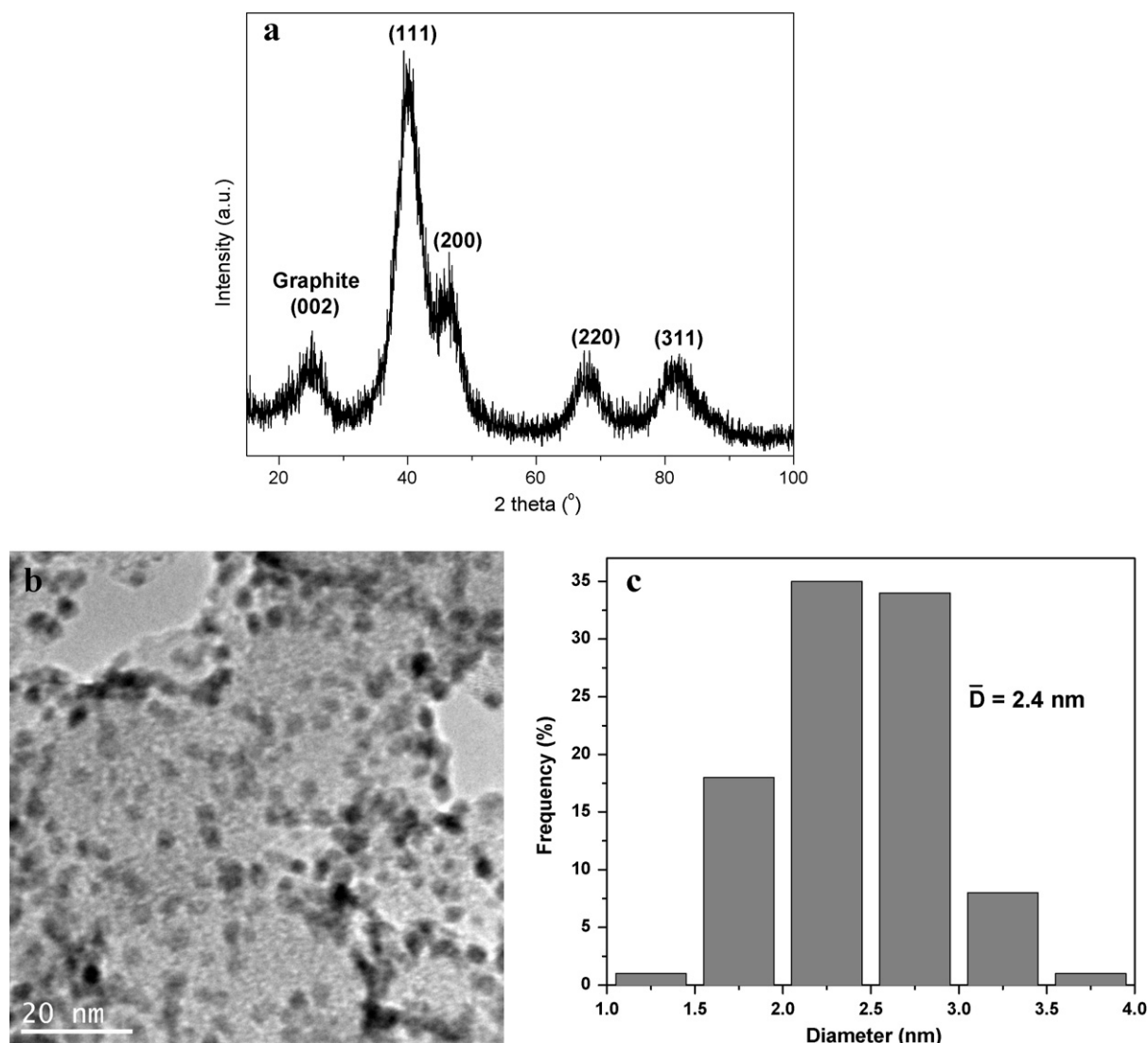
Fig. 1. (a) XRD pattern, (b) TEM image, and (c) particle size distribution of Pt/C catalyst.

a self-designed needle that was positioned within 0.5 mm to the center of working electrode surface. Before collection, the needle was washed with copious amounts of de-ionized water. The collection rate was controlled at 50 μl min⁻¹ by a peristaltic pump (Gilson minipuls 3). At each potential, 0.5 ml sample was collected and stored in a 2 ml screw cap vial (Agilent).

2.5. Products analysis

The product analysis was carried out using an HPLC (Agilent 1100) with a refractive index detector (RID, G1326A, Agilent). 20 μl of the sample was injected into the HPLC system and was separated using an OA-1000 column (Alltech) at 60 °C with an eluent of 5 mM aqueous sulfuric acid. Products were identified by comparison with authentic samples.

3. Results and discussions

3.1. Catalyst characterization

The XRD pattern of Pt/C catalyst is shown in Fig. 1a, which displayed a typical face-centered cubic (FCC) pattern. The average metal crystal size of Pt/C catalyst calculated based on the Pt (2 2 0)

diffraction peak is 1.9 nm, using the Debye–Scherrer formula shown below [51,56]:

$$L = \frac{0.9\lambda_{K\alpha}}{B_{2\theta}\cos\theta_{max}}$$

where L is the mean crystal size, λ is the wavelength of the X-ray (1.5406 Å), B is the full width at half-maximum of the peak (rad) and θ_{max} is the Bragg angle (rad) of Pt (2 2 0).

A typical TEM image of Pt/C and its corresponding histogram are shown in Fig. 1b. It is observed that most of the nanoparticles are round in shape and are uniformly dispersed on carbon support with only few agglomerations. The average particle size evaluated from the TEM image is 2.4 nm for Pt/C catalyst, which is in good agreement with the XRD result. The histogram of particle sizes (Fig. 1c) counted from 100 randomly chosen particles in an arbitrary area shows a narrow size distribution of 1–4 nm.

3.2. Electricity generation performance of anion-exchange membrane direct glycerol fuel cells (AEM-DGFCs)

Pt/C has demonstrated high activity towards electrocatalytic oxidation of glycerol in AEM-DGFC. As shown in Fig. 2, fed with an anode fuel of 2.0 M KOH + 1.0 M glycerol, the AEM-DGFC with an
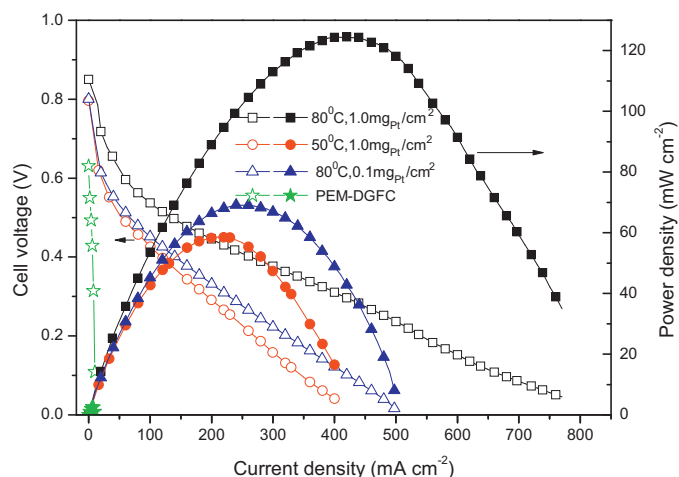
Fig. 2. Polarization curves of AEM-DGFC at operation temperature of 50 °C and 80 °C. Anode: Pt/C (40 wt%), 1.0 mg$_{Pt}$ cm^{-2}, or Pt/C (5 wt%), 0.1 mg$_{Pt}$ cm^{-2}; cathode: Fe-Cu-N$_4$/C (Acta 4020) 1.0 mg cm^{-2}, membrane: Tokuyama A201, 28 μm. 2.0 M KOH + 1.0 M glycerol. O$_2$: 0.4 l min^{-1}, 30 psi. PEM-DGFC: Anode: PtRu/C (4.0 mg$_{PtRu}$ cm^{-2}), cathode: Pt/C (4.0 mg$_{Pt}$ cm^{-2}), membrane: Nafion 115.

anode catalyst loading of 1.0 mg$_{Pt}$ cm^{-2} yields an open circuit voltage (OCV) of 0.796 V and a peak power density of 58.6 mW cm^{-2} at 50 °C. At a higher temperature of 80 °C, the OCV and peak power density can reach to 0.850 V, 124.5 mW cm^{-2}, respectively, due to the benefits of better reaction kinetics and fuel diffusion. We further reduced the anode catalyst loading to 0.1 mg$_{Pt}$ cm^{-2} with Pt/C (4.6 wt%) and observed that the peak power density of AEM-DGFC remains 69.1 mW cm^{-2} at 80 °C. The demonstrated power density represents 2–3 orders of magnitude higher than that of the current biofuel cells [57,58], and is also higher than the published results with Pd-based anode catalysts [39,44], which indicate Pt/C catalyst with small particles size (1–4 nm) possesses a high electrocatalytic activity toward glycerol oxidation in real fuel cell operations. In addition, the performance observed in AEMFC is over an order of magnitude higher than that of proton exchange membrane-direct glycerol fuel cell (PEM-DGFC) with the PtRu/C anode and Pt/C cathode catalysts with heavy loadings (8.0 mg$_{PGM}$ cm^{-2}$_{MEA}$). The comparison of electrocatalytic activity of glycerol oxidation using anion-exchange membrane (alkaline media) and proton-exchange membrane (acid media) is consistent with the results found in heterogeneous catalysis: the glycerol oxidation will be facilitated in high OH$^-$ concentrations [9,23].

3.3. Electrocatalytic oxidation of glycerol in AEM-DGFCs

3.3.1. Cogeneration of electricity and higher-valued chemicals

To investigate the cogeneration of electricity and valuable products on Pt/C in AEM-DGFC, 55 ml 2.0 M KOH + 1.0 M glycerol was continuously looped from an anode fuel vessel into the anode for 2 h. The fuel cell operation voltage was controlled at 0.7, 0.5, 0.3, and 0.1 V, to represent the operation in the close OCV, high working voltage, high power density and high current density conditions. As summarized in Fig. 3a and Table 1, the average power density and current density (within 2 h) are 6.6 mA cm^{-2} and 4.5 mW cm^{-2}, 50.0 mA cm^{-2} and 25.0 mW cm^{-2}, 158.9 mA cm^{-2} and 47.6 mW cm^{-2}, and 326.3 mA cm^{-2} and 32.5 mW cm^{-2}, for fuel cell operation voltage at 0.7, 0.5, 0.3, and 0.1 V, respectively. The average power density and current density are slightly lower than the values shown in Fig. 2 (regular I–V scan with open fuel-feeding), because the glycerol concentration gradually decreased during the long reaction time (2 h), due to cycled fuel-feeding. The high and stable AEMFC performance further suggests that fast kinetics of
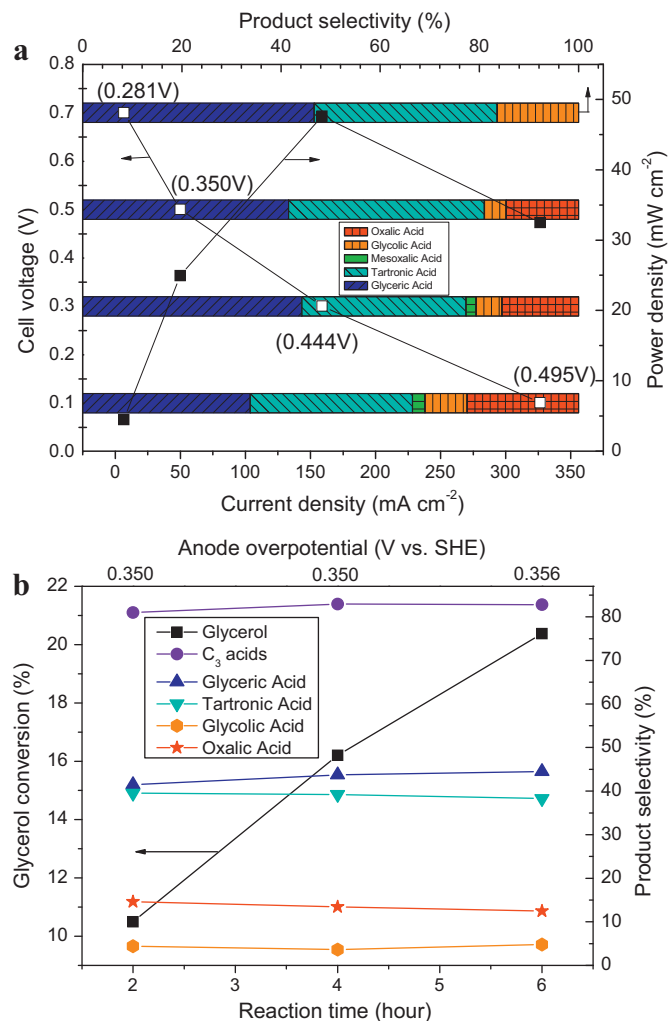

Fig. 3. (a) Electricity generation and products distribution from electrocatalytic oxidation of glycerol in AEMFC with 2.0 M KOH + 1.0 M glycerol at cell operation voltage at 0.7, 0.5, 0.3 and 0.1 V with an operation duration of 2 h at 50 °C, anode overpotential (vs. SHE) marked in parenthesis; (b) products distribution with different operation duration at the cell operation voltage of 0.5 V.

glycerol oxidation is not necessarily associated with complete oxidation of glycerol to CO$_2$ (as what has been achieved in biofuel cells).

The products were collected after 2 h of reaction and analyzed by HPLC. The selectivity is defined as the moles of product divided by the moles of C$_2$ and C$_3$ products observed at that time [23,59]. The oxidation products distributions under different operation voltages are summarized in Fig. 3a and Table 1. Traditional heterogeneous catalysis of glycerol oxidation in basic environment has been inefficient in the generation of deeper-oxidized C$_3$ acids (tartronic acid and mesoxalic acid). Tartronic acid selectivity is normally <7% on Pt/C catalyst in traditional batch reactors with a OH$^-$:glycerol ratio of 2:1 [7,23]. Even at an extremely high glycerol:catalyst ratio of 100:1 (mol mol^{-1}), the tartronic acid selectivity in batch reactor is still lower than 30% [7]. Although a high selectivity of mesoxalic acid of 70% is reported by oxidizing tartronic acid in acid (pH 1.5) [60], to the best of our knowledge, no mesoxalic acid has ever been reported on metallic catalysts in basic environment batch reactor operations, due to low reactivity of the secondary hydroxyl. However, different from the traditional catalytic oxidation of glycerol in batch reactor, the fuel cell reactor uniquely facilitates deeper-oxidized C$_3$ acids. The selectivity of tartronic acid can reach around 33–39% in the whole fuel cell operation voltage range. In addition, it

Table 1
Electro-oxidation of glycerol over Pt/C in AEM-DGFC with different base/glycerol concentrations at different fuel cell operation voltages.

	Cell voltage (V)	Selectivity (%)						Glycerol conversion (%)	Current density (mA cm^{-2})	Power density (mW cm^{-2})
		C$_3$ acids	Glyceric acid	Tartronic acid	Mesoxalic acid	Glycolic acid	Oxalic acid			
2.0 M KOH + 1.0 M glycerol	0.7	84	47	37	0	16	0	4.4	6.6	4.5
	0.5	81	41	40	0	4	15	10.5	50.0	25.0
	0.3	79	44	33	2	5	16	21.5	158.9	47.6
	0.1	70	34	33	3	8	22	37.1	326.3	32.5
4.0 M KOH + 1.0 M glycerol	0.7	83	46	37	0	17	0	3.1	6.7	4.5
	0.5	87	41	45	1	5	8	10.7	53.7	26.8
	0.3	85	40	42	3	5	10	23.7	195.0	58.4
0.5 M KOH + 1.0 M glycerol	0.7	78	44	34	0	22	0	0.6	1.9	1.3
	0.5	71	38	33	0	15	14	3.1	17.9	8.9
	0.3	70	49	21	0	13	17	9.9	69.3	20.8
2.0 M KOH + 0.1 M glycerol	0.7	91	41	50	0	9	0	4.7	1.1	0.7
	0.5	76	40	36	0	8	16	14.8	15.4	7.7
	0.3	62	21	34	7	10	28	63.7	56.7	17.0

is interesting to find that at the fuel cell operation voltage of <0.3 V, 2–3% of mesoxalic acid was collected in the AEMFC anode. The high selectivity of tartronic acid, together with the existence of fully oxidized C$_3$ acid, mesoxalic acid, strongly suggests that AEM-DGFC has unique ability to facilitate deeply oxidizing glycerol without breaking C—C bonds, as compared with glycerol oxidation in traditional heterogeneous catalytic batch reactors. In addition, more electrons transferred in producing deeper-oxidized products leads to a higher Faradic efficiency of fuel cell operation. For instance, the Faradic efficiency of glycerol oxidation to mesoxalic acid is 71% (10/14), which is higher than the Faradic efficiency of 29% (4/14) for glycerol oxidation to glyceric acid product.

On the other hand, the results clearly show the fuel cell operation voltage has an ability to control the product distribution: as the fuel cell voltage reduces, a clear trend of C$_3$ product selectivity drop has been observed from 84% to 70%. Moreover, the fuel cell voltage also affected the C$_2$ product selectivity. At the cell voltage of 0.7 V, the only C$_2$ product was glycolic acid (16%). With the operation voltage decreasing to 0.5 V, the main C$_2$ product was oxalic acid (15%). As the fuel cell voltage operated at 0.1 V, the selectivity of main product oxalic acid further increased to 22%. To investigate the effects of fuel cell operation voltage on the product selectivity, a Hg/HgO/1.0 M KOH electrode was used to on-line monitor the anode overpotential, which are 0.281, 0.350, 0.444, and 0.495 V vs. SHE for the fuel cell operation voltage at 0.7, 0.5, 0.3 and 0.1 V, respectively. The higher potential (electrical energy) applied on the anode obviously leads to deeper oxidations of glycerol, resulting in the formation of more oxalic acid and mesoxalic acid. Thus, it provides a feasible way to tune the product distributions though controlling the cell operation voltage (anode overpotential).

To further study the voltage effect on catalyst selectivity, 55 ml 2.0 M KOH + 1.0 M glycerol solution was cycled into the anode for a longer reaction time (6 h) at the cell voltage of 0.5 V. It can be seen from Table 2 that while glycerol conversion increased linearly during the entire test duration, the current density and power density decreased linearly due to the decreasing glycerol concentration. However, as shown in Fig. 3b, the anode overpotential was stable in the range of 0.350–0.356 V, indicating that the anode

overpotential could be controlled by regulating the fuel cell operation voltage. During the test, a 0.5 ml sample was taken from the system every 2 h for products analysis. The results as a function of time are shown in Fig. 3b. All product selectivity kept almost constant with time, and no mesoxalic acid or other products were found in the system at the fuel cell voltage of 0.5 V in the whole 6 h operation. This strongly indicated that the product selectivity could be well controlled by the cell operation voltage (anode overpotential).

After 6 h test, the volume of the electrolyte slightly increased to ~56 ml, which is higher than the original volume of 55 ml, due to the continuous generation of H$_2$O at the anode during the test. The glycerol and oxidation products trapped in the reaction system (mainly in catalyst layer and diffusion layer) were collected by flushing with de-ionized water until the OCV dropped to 0.01 V. The overall carbon balance is calculated by the following equation:

$$\text{Carbon balance} = \frac{3M_{Gi} - 3M_{C_3} - 2M_{C_2} - M_{C_1} - 3M_{Gf}}{3M_{Gi}} \times 100\%$$

where M_{Gi} and M_{Gf} are the initial and final moles of glycerol in the electrolyte, M_{C_3}, M_{C_2}, and M_{C_1} are the moles of C$_3$ products (glyceric acid, tartronic acid, and mesoxalic acid), C$_2$ products (glycolic acid and oxalic acid), and C$_1$ products (formic acid and carbonic acid), respectively. Assuming that no C$_2$ product was further oxidized to C$_1$ product, M_{C_2} is equal to M_{C_1}. Therefore, the equation can be simplified as:

$$\text{Carbon balance} = \frac{M_{Gi} - M_{C_3} - M_{C_2} - M_{Gf}}{M_{Gi}} \times 100\%$$

M_{C_3}, M_{C_2} and M_{Gf} include the amount of trapped chemicals. By this method, the carbon balance for the AEM-DGFC operated at a voltage of 0.5 V, 6 h is 6.5%. The carbon balances for the AEM-DGFC operation voltage at 0.7, 0.3, and 0.1 V are 4.3%, 14.0%, and 26.1%, respectively. The carbon balance is high at low fuel cell voltage, indicating some C$_2$ products (glycolic acid and oxalic acid) may be further oxidized to C$_1$ products (formic acid or carbonic acid) on the highly active Pt/C catalyst.

Table 2
Electro-oxidation of glycerol over Pt/C in AEM-DGFC with 2.0 M KOH + 1.0 M glycerol at the fuel cell voltage of 0.5 V for different time.

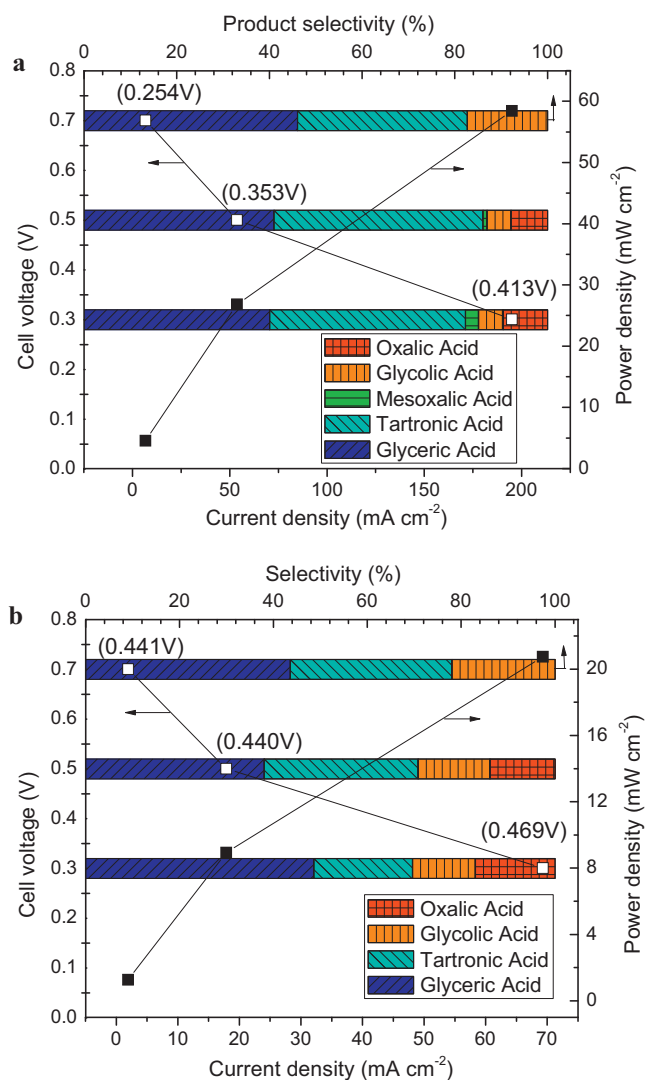| Reaction duration (h)	Selectivity (%)						Glycerol conversion (%)	Current density (mA cm^{-2})	Power density (mW cm^{-2})
	C$_3$ acids	Glyceric acid	Tartronic acid	Mesoxalic acid	Glycolic acid	Oxalic acid			
2	81	41	40	0	4	15	10.5	50.0	25.0
4	83	44	39	0	4	13	16.2	43.9	21.9
6	83	45	38	0	5	12	20.4	38.6	19.3

Fig. 4. Electricity generation and product distribution from electrocatalytic oxidation of glycerol in AEMFC with 1.0 M glycerol + (a) 4.0 M KOH and (b) 0.5 M KOH fuel for an operation duration of 2 h at 50 °C, anode overpotential (vs. SHE) marked in parenthesis.

3.3.2. Effects of base concentration

To evaluate the KOH effects, 1.0 M glycerol mixed with 4.0 M or 0.5 M KOH as fuel was cycled into the anode for 2 h, and the results are shown in Fig. 4. Comparison between Fig. 3a and Fig. 4 reveals that higher KOH concentration will lead to higher electricity generation performance. The average power density at 0.3 V with 4.0 M KOH + 1.0 M glycerol is 58.4 mW cm^{-2}, which is almost three times of that with 0.5 M KOH + 1.0 M glycerol (20.8 mW cm^{-2}). This can be attributed to the following reasons. First, the higher OH^{-} concentration will improve OH^{-} diffusion at the anode, thus, increasing the fuel cell electricity performance [61]. Second, according to the bi-functional theory, the oxidation of alcohol is governed by the coverage degree of both –RO$_{ads}$ and OH$_{ads}$. High OH^{-} concentration in bulk electrolyte will increase OH$_{ads}$ on Pt catalyst surface. Third, it was reported that high pH would benefit the initial dehydrogenation of alcohol [59]. Therefore, high OH^{-} concentration will promote the generation of alkoxy intermediate adsorbed on Pt catalyst surface by lowing the activation energy barrier [23]. As a result, faster reaction kinetics will be achieved in a higher pH electrolyte. This is evidenced by the lower anode overpotential observed in a higher KOH concentration electrolyte.
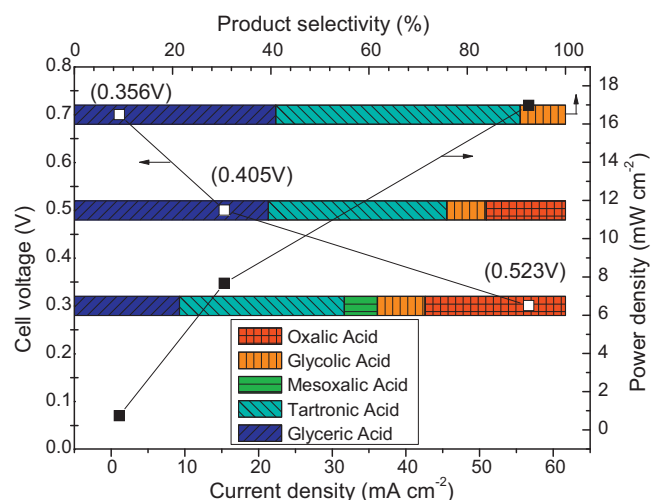

Fig. 5. Electricity generation and product distribution from electrocatalytic oxidation of glycerol in AEMFC with 2.0 M KOH + 0.1 M glycerol as the fuel for an operation duration of 2 h at 50 °C, anode overpotential (vs. SHE) marked in parenthesis.

As the O—H bond activation barrier is greatly reduced in high pH media [23], it is more favorable to oxidize hydroxyl group to carboxyl other than break C—C bond. Therefore, higher concentrations of KOH have been found to slightly benefit the C$_3$ acids formation. When 0.5 M KOH was used (Fig. 4b), the C$_3$ acids selectivity varies from 70% to 78% with the fuel cell voltage from 0.7 to 0.3 V. As KOH concentration increased to 2.0 M (Fig. 3a), the C$_3$ acids selectivity is 79–84%. When the KOH increased to 4.0 M (Fig. 4a), the C$_3$ acids selectivity is 83–87%. As the O—H bond activation barrier drops in higher pH media, mesoxalic acid production, which requires the oxidation of the secondary hydroxyl, was observed even at the operation voltage of 0.5 V in the 4.0 M KOH + 1.0 M glycerol test. On the contrary, when 0.5 M KOH + 1.0 M glycerol was used, no mesoxalic acid was collected even at 0.3 V operation voltage, indicating a strong KOH concentration effect on the product selectivity.

3.3.3. Effects of glycerol concentration

Since glycerol oxidation is related to both –RO$_{ads}$ and OH$_{ads}$ coverage degree on the Pt catalyst surface, when glycerol concentration decreasing from 2.0 M to 0.1 M, both the current density and power density remarkably decreased, and the anode overpotential shifted positively. As shown in Fig. 5 and Table 1, glycerol concentration strongly affects the glycerol conversion rate. Due to the reduced amount (concentration) of glycerol, glycerol conversion in 2.0 M KOH + 0.1 M glycerol is higher than that obtained in 2.0 M KOH + 1.0 M glycerol. This is especially apparent at a fuel cell operation voltage of 0.3 V, where the glycerol conversion could reach 63.7%, which is three times of that observed in 1.0 M glycerol (21.5%). The limitation of fuel feeding also affects the product selectivity. At the cell voltage of 0.7 V, a high tartronic acid selectivity of 50% and a total C$_3$ acids selectivity of 91% were achieved. As the cell voltage decreased to 0.3 V, the total C$_3$ acids selectivity decreased to 62%, while the glyceric acid dropped to 21%. However in the meantime, very high mesoxalic acid and oxalic acid selectivities reached 7% and 28%, respectively. This indicates that with a low glycerol concentration, the high output power density at 0.3 V requires deeper oxidation of glycerol, resulting in high mesoxalic acid (fully oxidized C$_3$ acid) and oxalic acid (fully oxidized C$_2$ acid) selectivities.

3.3.4. Reaction stability test

The reaction stability of Pt/C catalyst was tested through 10 runs of 2-h-operation of glycerol oxidation with 2.0 M KOH + 1.0 M
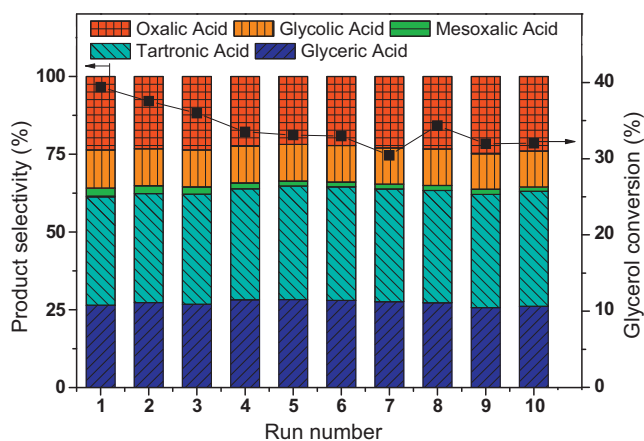
Fig. 6. Reaction stability of Pt/C catalyst in AEM-DGFC with 2.0 M KOH + 1.0 M glycerol at the cell operation voltage of 0.1 V, cathode: Fe-Cu-N$_4$/C (Acta 4020), 1.3 mg cm^{-2}, run time: 2 h, 10 runs, 50 °C.

glycerol under the same test conditions (Fig. 6). The fuel cell operation voltage was kept at 0.1 V, at which the anode catalyst suffers the highest overpotential and the fuel cell generates the highest current density. The cathode catalyst loading was increased to 1.3 mg cm^{-2} to minimize the effect of cathode catalyst activity loss. After each run, the anode was cleaned by flushing with de-ionized water until the OCV dropped down to <0.01 V. As shown in Fig. 6, the selectivity to each product kept almost constant during the 10 runs of stability tests, which demonstrates stable catalyst selectivity on the Pt/C during the repetitive operations. In the meantime, the Pt/C also presents a high stability against deactivation. The glycerol conversion dropped from 39.4% to 37.6% after the first run, and was stabilized at 32–33% after four consecutive runs. The Pt/C catalyst maintained 81.2% of its initial catalyst activity after 10 runs (a total 20 h operation), indicating an excellent stability and reusability of the Pt/C for anode catalyst of the AEM-DGFC.

3.4. Reaction sequence of electro-oxidation of glycerol on Pt/C in half cell

The combination of half cell voltammetry techniques with HPLC analysis to study the kinetics and mechanism of glycerol electro-oxidation was reported by Lamy's group in 1990s. However, due to the large gap in timescales of these two analysis method, Lamy's early research is limited to studying reaction products in long-time electrolysis [41]. Recently, Koper's group developed an on-line collection off-line HPLC analysis system, through which the glycerol electro-oxidation products on polycrystalline Pt and Au electrode surface were continuously collected under different potentials during a linear voltammetry scan in dilute glycerol solution (e.g. 0.1 M NaOH + 0.1 M glycerol), and analyzed thereafter by HPLC [53,55]. In light of Koper's work, we designed a similar sample collection set-up, and employed it in linear staircase scans on supported Pt nanoparticle catalyst in both 0.1 M KOH + 0.1 M glycerol and 1.0 M KOH + 1.0 M glycerol, with a potential increment of 100 mV 10 min^{-1}. Our goal was to investigate the reaction sequence of glycerol oxidation on supported Pt catalysts with high concentration fuel solution.

The polarization curves are shown in Fig. 7a. The current generation started at 0.4 V, with a peak current at 1.1 V in 0.1 M KOH + 0.1 M glycerol. A steep drop in current density was observed at potential >1.1 V, which is due to the deactivation caused by the oxidation of surface Pt. When the concentration of KOH and glycerol increased to 1.0 M, the onset potential negatively shifted to 0.2 V, while the peak current density increased to 33.4 mA cm^{-2}, which is
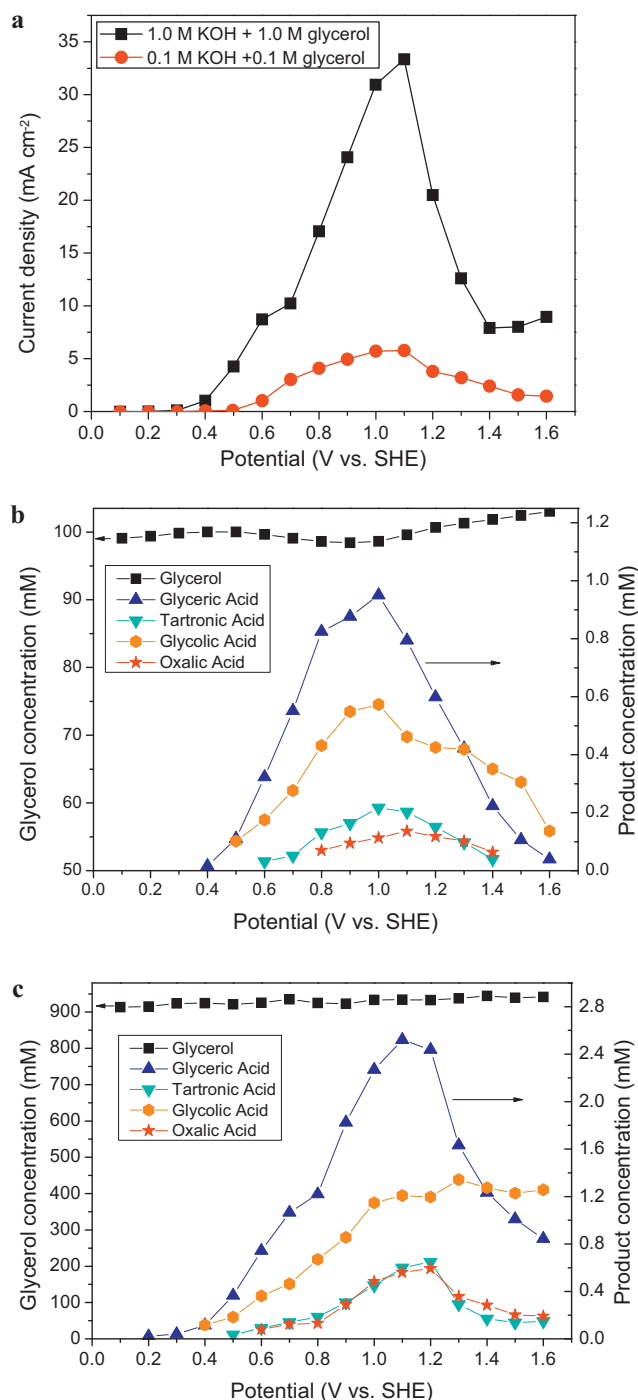

Fig. 7. Electrocatalytic oxidation of glycerol on Pt/C catalyst: (a) polarization curves in 0.1 M KOH + 0.1 M glycerol and 1.0 M KOH + 1.0 M glycerol, and oxidation products concentration profiles in (b) 0.1 M KOH + 0.1 M glycerol and (c) 1.0 M KOH + 1.0 M glycerol, room temperature.

six times higher than that evidenced in 0.1 M KOH + 0.1 M glycerol (5.8 mA cm^{-2}). This indicated higher kinetics could be achieved in higher KOH and glycerol concentrations, which is in good agreement with the single AEMFC results.

The oxidation products under each applied potential were collected by a needle positioned within 0.5 mm to the center of the working electrode with a collection rate of 50 μl min^{-1}. The products in each sample were separated by HPLC column, and identified by comparing their retention times with the authentic samples. The product concentration was calculated from the peak area

observed in liquid chromatograms. The concentration profiles for 0.1 M KOH + 0.1 M glycerol and 1.0 M KOH + 1.0 M glycerol are summarized in Fig. 7b and c, respectively. Because only small amount of catalyst was deposited on the glassy carbon electrode, the diffusion issue is negligible as compared with that in single cell. Therefore, the samples collected from the half cell could be used to present the instantaneous products concentration around the catalyst surface. As shown in Fig. 7b, the oxidation products were detected in the sequence of glyceric acid, glycolic acid, tartronic acid, and oxalic acid. This observation agrees with the results on polycrystalline platinum disk recently studied by Koper's group, [53] indicating that glycerol oxidation sequence on supported Pt nanoparticle catalyst is similar to that on the bulk polycrystalline platinum electrode. The products sequence in the half cell is also in agreement with the products distribution examined from the fuel cell reactor, where oxalic acid is the product that was not found at relatively low anode overpotential. The product concentration profile in Fig. 7b shows a volcano shape on each product, with glyceric acid having the highest concentration in low potentials. However, different from what Kwon has reported, at potentials >1.3 V, the concentration of glycolic acid in the collected samples exceeded that of glyceric acid, suggesting that the C—C bond cleavage dominates on the PtO surface.

As both KOH and glycerol concentrations increased to 1.0 M, the products concentration profile is shown in Fig. 7c. It is interesting that the oxidation products were detected in the same sequence as that in 0.1 M KOH + 0.1 M glycerol. However, the initial detected potential for each product moved negatively, while the product concentration collected at each potential increased significantly, indicating higher catalyst reactivity achieved in a concentrated electrolyte. The effect of fuel concentration has also been observed in AEM-DGFC tests: at high concentrations of glycerol or KOH, the anode overpotential decreased and the power density increased.

However, there are still some inconsistencies between these two electrocatalytic reaction systems. In the AEM-DGFC test with 2.0 M KOH + 1.0 M glycerol, tartronic acid and oxalic acid were observed at anode overpotential of 0.281 and 0.350 V vs. SHE, respectively. These anode overpotentials are much lower than the 'initial' detected potentials in half cell (tartronic acid at 0.5 V, oxalic acid at 0.6 V, vs. SHE, in 1.0 M KOH + 1.0 M glycerol). At the same time, the concentration of tartronic acid in the AEM-DGFC is much higher than that in the half cell. No mesoxalic acid was detected in our half cell tests, nor in previous published work by FTIR [62] and HPLC [53,55]. Three possible reasons may explain these discrepancies. First, the molar ratio of glycerol to catalyst in the AEM-DGFC (2.0 M NaOH + 1.0 M glycerol) is 2146:1 (mol:mol), which is 57 times smaller than the ratio in the half cell test in 1.0 M KOH + 1.0 M glycerol (121,928:1). The higher catalyst loading in AEM-DGFC leads to a thicker catalyst layer and causes some diffusion difficulty. Therefore, some glycerol and glycerol oxidation intermediates could be trapped in the diffusion and catalyst layers, which may lead to formation of deeper-oxidized products, i.e. tartronic acid and mesoxalic acid. The deeper-oxidized product tartronic acid has also been reported in previous publication of electrolysis of glycerol, in which a glycerol to catalyst ratio similar to ours was used [63]. Second, the product concentration profile obtained from the half cell tests represents the instantaneous local products concentration around the Pt catalyst, which is not an equilibrated product distribution. However, the products distribution in the AEM-DGFC is the stable bulk concentration after a long reaction time. Third, the tartronic acid was produced much greater in the AEM-DGFC than in the half cell. As shown in Fig. 5, increasing the base concentration will lead to the products generated at a lower potential. Therefore, when the KOH concentration further increases to 2.0 M, it is possible that these deeper-oxidized products are generated on dense catalyst nanoparticles at an even lower potential.

Higher concentration of tartronic acid will lead to its further oxidation to mesoxalic acid in the AEM-DGFC reaction environment. The inconsistencies between these two systems imply that glycerol oxidation reactors and processes may strongly influence the products distribution. The unique catalytic environment in AEM-DGFC may offer unique opportunities to selectively generate deeper-oxidized products, which have not been detected in previous half cell tests, and are difficult to be produced through heterogeneous catalytic oxidation processes in batch reactors. In order to acquire better understanding of the glycerol electro-oxidation mechanisms in AEM-DGFC, research on designing model electrolysis cells with on-line product collection and on-site characterization are needed, and currently underway in our lab.

4. Conclusions

In summary, a solution phase-based nanocapsule method was used to prepare Pt/C catalysts with a small diameter of 2.4 nm and a narrow size distribution of 1–4 nm. The Pt/C catalyst has demonstrated unique electrocatalytic function towards cogeneration of both electricity (124.5 mW cm^{-2} at 80 °C) and valuable chemicals (91% C$_3$ acids selectivity at 0.7 V, 2.0 M KOH + 0.1 M glycerol), as well as excellent stability in AEM-DGFC. Compared to heterogeneous catalytic oxidation of glycerol in traditional batch reactors, our study showed unique fuel cell operation voltage (anode overpotential) regulated product distributions: high tartronic acid selectivity (50% at 0.7 V, 2.0 M KOH + 0.1 M glycerol). In addition, the fully oxidized C$_3$ acid- mesoxalic acid with the highest selectivity of 7% (0.3 V, 2.0 M KOH + 0.1 M glycerol) was first reported on metallic catalyst in high pH media. The reaction mechanism study based on glycerol oxidation in half-cell using an online collection, offline HPLC analysis technique indicates a similar glycerol oxidation sequence as revealed in AEM-DGFC. However, the inconsistencies between the two systems still exist, possibly due to the quite different reaction environments, such as electrode structure, glycerol:catalyst ratio, and residence time of reactants.

References

[1] A. Corma, S. Iborra, A. Velty, Chem. Rev. 107 (2007) 2411–2502.
[2] T.P. Vispute, H.Y. Zhang, A. Sanna, R. Xiao, G.W. Huber, Science 330 (2010) 1222–1227.
[3] L.R. Lynd, M.S. Laser, D. Brandsby, B.E. Dale, B. Davison, R. Hamilton, M. Himmel, M. Keller, J.D. McMillan, J. Sheehan, C.E. Wyman, Nat. Biotechnol. 26 (2008) 169–172.
[4] B. Katryniok, H. Kimura, E. Skrzynska, J.-S. Girardon, P. Fongarland, M. Capron, R. Ducoulombier, N. Mimura, S. Paul, F. Dumeignil, Green Chem. 13 (2011) 1960–1979.
[5] M. Pagliaro, R. Ciriminna, H. Kimura, M. Rossi, C. Della Pina, Angew. Chem. Int. Ed. 46 (2007) 4434–4440.
[6] C.H.C. Zhou, J.N. Beltramini, Y.X. Fan, G.Q.M. Lu, Chem. Soc. Rev. 37 (2008) 527–549.
[7] S. Carrettin, P. McMorn, P. Johnston, K. Griffin, C.J. Kiely, G.J. Hutchings, Phys. Chem. Chem. Phys. 5 (2003) 1329–1336.
[8] D. Hekmat, R. Bauer, Biotechnol. Prog. 22 (2006) 278–284.
[9] R. Garcia, M. Besson, P. Gallezot, Appl. Catal. A 127 (1995) 165–176.
[10] P. Gallezot, Catal. Today 37 (1997) 405–418.
[11] C.L. Bianchi, P. Canton, N. Dimitratos, F. Porta, L. Prati, Catal. Today 102 (2005) 203–212.
[12] J. Gao, D. Liang, P. Chen, Z.Y. Hou, X.M. Zheng, Catal. Lett. 130 (2009) 185–191.
[13] D. Liang, J. Gao, J.H. Wang, P. Chen, Z.Y. Hou, X.M. Zheng, Catal. Commun. 10 (2009) 1586–1590.
[14] N. Dimitratos, F. Porta, L. Prati, Appl. Catal. A 291 (2005) 210–214.
[15] M. Sankar, N. Dimitratos, D.W. Knight, A.F. Carley, R. Tiruvalam, C.J. Kiely, D. Thomas, G.J. Hutchings, ChemSusChem 2 (2009) 1145–1151.

[16] S. Carrettin, P. McMorn, P. Johnston, K. Griffin, G.J. Hutchings, Chem. Commun. (2002) 696–697.
[17] F. Porta, L. Prati, J. Catal. 224 (2004) 397–403.
[18] S. Carrettin, P. McMorn, P. Johnston, K. Griffin, C.J. Kiely, G.A. Attard, G.J. Hutchings, Top. Catal. 27 (2004) 131–136.
[19] A. Abad, P. Concepción, A. Corma, H. García, Angew. Chem. Int. Ed. 44 (2005) 4066–4069.
[20] M.D. Hughes, Y.-J. Xu, P. Jenkins, P. McMorn, P. Landon, D.I. Enache, A.F. Carley, G.A. Attard, G.J. Hutchings, F. King, E.H. Stitt, P. Johnston, K. Griffin, C.J. Kiely, Nature 437 (2005) 1132–1135.
[21] A. Villa, D. Wang, D.S. Su, L. Prati, ChemCatChem 1 (2009) 510–514.
[22] A. Villa, A. Gaiassi, I. Rossetti, C.L. Bianchi, K. van Benthem, G.M. Veith, L. Prati, J. Catal. 275 (2010) 108–116.
[23] B.N. Zope, D.D. Hibbitts, M. Neurock, R.J. Davis, Science 330 (2010) 74–78.
[24] A. Villa, G.M. Veith, L. Prati, Angew. Chem. Int. Ed. 49 (2010) 4499–4502.
[25] E.G. Rodrigues, M.F.R. Pereira, X. Chen, J.J. Delgado, J.J.M. Orfao, J. Catal. 281 (2011) 119–127.
[26] A.N. Grace, K. Pandian, Electrochem. Commun. 8 (2006) 1340–1348.
[27] Y.H. Shen, S.H. Zhang, H.J. Li, Y. Ren, H.C. Liu, Chem. Eur. J. 16 (2010) 7368–7371.
[28] G.L. Brett, Q. He, C. Hammond, P.J. Miedziak, N. Dimitratos, M. Sankar, A.A. Herzing, M. Conte, J.A. Lopez-Sanchez, C.J. Kiely, D.W. Knight, S.H. Taylor, G.J. Hutchings, Angew. Chem. Int. Ed. 50 (2011) 10136–10139.
[29] N. Dimitratos, C. Messi, F. Porta, L. Prati, A. Villa, J. Mol. Catal. A: Chem. 256 (2006) 21–28.
[30] W. Ketchie, M. Murayama, R. Davis, J. Catal. 250 (2007) 264–273.
[31] N. Dimitratos, J.A. Lopez-Sanchez, J.M. Anthonykutty, G. Brett, A.F. Carley, R.C. Tiruvalam, A.A. Herzing, C.J. Kiely, D.W. Knight, G.J. Hutchings, Phys. Chem. Chem. Phys. 11 (2009) 4952–4961.
[32] N. Dimitratos, A. Villa, L. Prati, Catal. Lett. 133 (2009) 334–340.
[33] D. Wang, A. Villa, F. Porta, L. Prati, D.S. Su, J. Phys. Chem. C 112 (2008) 8617–8622.
[34] W.B. Hu, D. Knight, B. Lowry, A. Varma, Ind. Eng. Chem. Res. 49 (2010) 10876–10882.
[35] W. Hu, B. Lowry, A. Varma, Appl. Catal. B 106 (2011) 123–132.
[36] D. Liang, J. Gao, J. Wang, P. Chen, Y. Wei, Z. Hou, Catal. Commun. 12 (2011) 1059–1062.
[37] M. Simões, S. Baranton, C. Coutanceau, Appl. Catal. B 110 (2011) 40–49.
[38] M. Besson, P. Gallezot, Catal. Today 57 (2000) 127–141.
[39] C. Bianchini, P.K. Shen, Chem. Rev. 109 (2009) 4183–4206.
[40] E.H. Yu, U. Krewer, K. Scott, Energies 3 (2010) 1499–1528.
[41] L. Roquet, E.M. Belgsir, J.M. Leger, C. Lamy, Electrochim. Acta 39 (1994) 2387–2394.
[42] M. Simoes, S. Baranton, C. Coutanceau, Appl. Catal. B 93 (2010) 354–362.
[43] K. Matsuoka, Y. Iriyama, T. Abe, M. Matsuoka, Z. Ogumi, J. Power Sources 150 (2005) 27–31.
[44] V. Bambagioni, C. Bianchini, A. Marchionni, J. Filippi, F. Vizza, J. Teddy, P. Serp, M. Zhiani, J. Power Sources 190 (2009) 241–251.
[45] A. Ilie, M. Simoes, S. Baranton, C. Coutanceau, S. Martemianov, J. Power Sources 196 (2011) 4965–4971.
[46] W.Z. Li, Z.W. Chen, L.B. Xu, Y. Yan, J. Power Sources 195 (2010) 2534–2540.
[47] W.Z. Li, P. Haldar, Electrochem. Solid-State Lett. 13 (2010) B47–B49.
[48] W.Z. Li, P. Haldar, Electrochem. Commun. 11 (2009) 1195–1198.
[49] Z.Y. Zhang, M.J. Li, Z.L. Wu, W.Z. Li, Nanotechnology 22 (2011).
[50] Z.Y. Zhang, K.L. More, K. Sun, Z.L. Wu, W.Z. Li, Chem. Mater. 23 (2011) 1570–1577.
[51] Z.Y. Zhang, L. Xin, K. Sun, W.Z. Li, Int. J. Hydrogen Energy 36 (2011) 12686–12697.
[52] S.H. Sun, C.B. Murray, D. Weller, L. Folks, A. Moser, Science 287 (2000) 1989–1992.
[53] Y. Kwon, M.T.M. Koper, Anal. Chem. 82 (2010) 5420–5424.
[54] M.T.M. Koper, Y. Kwon, S.C.S. Lai, P. Rodriguez, J. Am. Chem. Soc. 133 (2011) 6914–6917.
[55] Y. Kwon, K.J.P. Schouten, M.T.M. Koper, ChemCatChem 3 (2011) 1176–1185.
[56] W.Z. Li, C.H. Liang, W.J. Zhou, J.S. Qiu, Z.H. Zhou, G.Q. Sun, Q. Xin, J. Phys. Chem. B 107 (2003) 6292–6299.
[57] R.L. Arechederra, B.L. Treu, S.D. Minteer, J. Power Sources 173 (2007) 156–161.
[58] R.L. Arechederra, S.D. Minteer, Fuel Cells 9 (2009) 63–69.
[59] W.C. Ketchie, M. Murayama, R.J. Davis, Top. Catal. 44 (2007) 307–317.
[60] P. Fordham, M. Besson, P. Gallezot, Catal. Lett. 46 (1997) 195–199.
[61] H. Bunazawa, Y. Yamazaki, J. Power Sources 182 (2008) 48–51.
[62] J. Gomes, G. Tremiliosi-Filho, Electrocatalysis 2 (2011) 96–105.
[63] V. Bambagioni, M. Bevilacqua, C. Bianchini, J. Filippi, A. Lavacchi, A. Marchionni, F. Vizza, P.K. Shen, ChemSusChem 3 (2010) 851–855.